JOURNAL OF PROPULSION AND POWER
Vol. 20, No. 5, September–October 2004

Oscillation Frequency in Wake of a Vee Gutter

Rong F. Huang* and Kuo T. Chang†
National Taiwan University of Science and Technology, Taipei 106, Taiwan, Republic of China

The oscillating behaviors and frequency selection of the unsteady flows in the wake of a vee gutter are studied experimentally in a wind-tunnel by the use of the smoke-wire flow visualization technique and the hot-wire anemometer. The effective length of the vee gutter is determined by the variation of vortex shedding frequency. The functional relationships of the dominant mechanisms in the limiting ranges of Reynolds number are justified by the arguments made on the Strouhal number and the Roshko number. The oscillating motions in the wake region of the vee gutter possess two types of instabilities: the high-frequency shear-layer instability waves and the low-frequency vortex shedding. Four characteristic modes of the shed vortices: laminar, subcritical, transitional, and supercritical, are identified according to the differences of their physical properties. Variations of the Strouhal numbers of the shear-layer instability waves and the vortex shedding are presented and discussed. Characteristic frequencies of the wakes behind various geometries and sharpness of trailing edges are compared.

Nomenclature

f	=	frequency of instabilities in wake region, Hz
L	=	span length of vee gutter
L_{eff}	=	Effective length of vee gutter
ℓ	=	characteristic length scale in x direction
Re_W	=	Reynolds number based on cross-stream width W of wing section, $U_\infty W/\nu$
Ro_W	=	Roshko number based on cross-stream width W of wing section, fW^2/ν
St_W	=	Strouhal number of vortex shedding, fW/U_∞
T	=	characteristic timescale
U_∞	=	freestream velocity
u	=	x component of local velocity
V	=	characteristic velocity scale in y direction
v	=	y component of local velocity
W	=	cross-stream width of vee gutter
X	=	streamwise coordinate originated from leading edge of vee gutter
x	=	streamwise coordinate
Y	=	spanwise coordinate originated from center of vee gutter span
y	=	cross-stream coordinate
Z	=	chordwise coordinate originated from leading edge of vee gutter
δ	=	characteristic length scale in y direction
θ	=	span angle of vee gutter
ν	=	kinetic viscosity of airstream

Introduction

IT has been widely acknowledged that the introduction of a bluff body into the airstream is an effective way of flame holding in many combustion apparatuses, for example, ramjet combustors, thrust augmenters, industrial burners, etc. Ample evidence has shown that aerodynamic characteristics of the near-wake flow behind a bluff body have a crucial influence on flame structures and flame-holding mechanisms. This type of flow is usually associated with complicated phenomena such as separation, recirculation, mass entrainment through the shear layers, and vortex shedding. The unsteady flow motions in the bluff-body wakes have been proven to be of profound influences on the mixing and combustion efficiency. In general, the mixing capability, heat transfer, and combustion efficiency can be notably enhanced through the strong cross-stream exchanges of the momentum and mass. Many of the detailed phenomena, however, have not yet been well understood. Hence, the average and dynamic wake structures, physical mechanisms, and applications have attracted the interest of many investigators during the past few decades. The shapes of the bluff bodies for flame-holding employed by the researchers were diverse, for instance, the circular cylinder,[1] flat plate,[2] circular disc,[3,4] half-triangular cylinder,[5,6] vee gutter or slit vee gutter,[7–9] etc.

The wake behind a body usually consists of the shear layer and/or the alternative vortex shedding, which is responsible for the periodic unsteady motions. Conventionally, research on the oscillating flows in the wakes was focused on the basic flows, such as the coherent structures behind a bluff body,[10–12] the wake behind the slender body with blunt trailing edge,[13,14] or the oscillations behind an airfoil.[15–18] Most wake oscillations behind a bluff body reported in the literature were commonly translated to an ordinary Strouhal number $St = fd/U_\infty$, where f is the flow oscillation frequency, d is the cross-stream length scale of the body, and U_∞ is the freestream velocity. Roshko[19] found that the ordinary Strouhal number remains near constant 0.21, 0.18, and 0.14 for a circular cylinder, 90-deg wedge, and bluff plate, respectively, for Reynolds numbers in the range between 10^3 and 10^5. Simons[20] further introduced a universal Strouhal number St^* based on the measured wake width d^* for the two-dimensional bluff bodies and found a constant value of $St^* = 0.163$. Roshko[19] also successfully applied the inviscid Kirchhoff free streamline theory to relate the drag and the universal Strouhal number by a k function, which implied the appropriation of the inviscid model in the bluff-body wake at large Reynolds numbers. Levi[21] justified the universal Strouhal law by modeling the available specific kinetic energy, $U_\infty^2/2$, of the oscillating fluids by the specific mechanical energy, $(2\pi f d^*)^2/2$, of the oscillator oscillating within the width d^* with a frequency f. The universal Strouhal number $St^* = 1/2\pi = 0.159$, which is very close to the experimental result of 0.163 of Simons,[20] was derived. Zaman et al.[22] reported that during the deep stall of an airfoil at angles of attack larger than 18 deg, the usual bluff-body shedding occurs at the ordinary Strouhal frequency 0.2 in the chord Reynolds number range from 0.15×10^5 to 3.0×10^5.

Because the viscous force is not negligible in the analysis of the evolving process of the instability waves at the initial stage of the spatially developing vortex street,[23] the frequency characteristics in a shear layer are different from that in a bluff-body wake. Nishioka and Sato[24] showed that the shedding frequency behind a circular cylinder at very low Reynolds numbers is determined by the selective linear growth of small fluctuations. At higher Reynolds

Received 27 August 2002; accepted for publication 22 January 2004.

*Professor, Department of Mechanical Engineering, 43 Keelung Road, Section 4; rfhuang@mail.ntust.edu.tw. Senior Member AIAA.

†Graduate Student, Department of Mechanical Engineering.

numbers, however, nonlinear effects dominate. Therefore, the dominant mechanisms of the unsteady motions of the shear-layer instabilities and the vortex shedding in the wake of a bluff body are inevitably different.

Although the flow characteristics of various bluff-body wakes have been comprehensively studied, literature on the detailed behaviors, dominant mechanisms, and frequency selection of the unsteady wake behind a vee gutter is limited. This study focuses on the frequency characteristics of the wake instabilities to understand the behavior and dominant mechanism of the vee-gutter wake. The experimental results of the frequency characteristics and various types of oscillation in a vee-gutter wake are presented. A similarity justification is conducted to assist in the interpretation of the experimental results and the dominant mechanisms.

Experimental Setup

The experiments were performed in an open-loop, low-speed wind tunnel with a honeycomb section, three wire-mesh screens, a 10:1 contractor, and a test section of $40.0 \times 25.0 \times 100$ cm, as shown in Fig. 1. Freestream turbulence intensity was lower than 0.4%, within the experimental range $U_\infty = 0.25 \sim 22$ m/s. (The Reynolds number based on W is between 4.6×10^2 and 4.1×10^4.) Nonuniformity of the average velocity profiles across the test section was lower than 0.5%. During the experiments, the average velocity of the approaching flow was constantly monitored with a retractable laser Doppler velocimetry-calibrated pitot-static tube, together with a calibrated Validyne pressure transducer. An acrylic vee gutter, as shown in Fig. 2, with a span angle $\theta = 90$ deg was installed horizontally at the symmetry plane of the test section. The distance between the vee gutter and the outlet of the wind-tunnel nozzle was 20 cm. Geometry of the vee gutter and the definition of the coordinates are shown in Fig. 2. The origin is located at the central vertex of the vee gutter. The coordinates X, Y, and Z denote the directions of the freestream, vee-gutter span, and cross-stream, respectively. Two cross-stream widths, $W = 18$ and 28 mm, were tested in this study. Because the two results are similar, only the latter is presented in this paper. The blockage ratio of the vee-gutter in the wind-tunnel test section is about 7 and 10% for the $W = 18$ and 28 mm vee-gutters, respectively. The thickness of the vee-gutter wings is 1 mm. The ends of the vee gutter were clamped with thin, sharp-edged square plates of 8-cm side length.

The smoke-wire technique was used to visualize the flow separation, as well as the vortex evolution for wind velocity lower than 3.2 m/s ($Re_W = 6 \times 10^3$). Photography was done via a high-speed charge-coupled device camera. Two corrugated wolfram wires with a diameter of 80 μm were used as the smoke wires. One of them was placed 20 mm upstream the leading edge of the vee gutter, and the other was situated 0.5 mm downstream the trailing edge. Thin mineral oil was brush-coated on the wire surface. The wire was electrically heated to generate fine smoke streaks, and made the flowfield observable. The surface temperature of the smoke wire was kept as low as possible, but high enough to evaporate the oil. The buoyancy-induced convection[25] was estimated to be lower than 2.5 cm/s. The condensed vapor aerosols (the "smoke") of the thin mineral oil had diameters on the order of 1 μm (Ref. 26). The slip factor and Stokes number[27] for these aerosols were estimated to be about 1.108 and 0.002, respectively. The smoke streaks, hence, were considered to be able to follow the flow appropriately.

The frequencies of the shed vortices in the wake region and the instability waves developed on the separated shear layers were detected by a homemade, constant-temperature, one-component hot-wire anemometer. The output signals of the hot-wire anemometer were fed simultaneously to a fast Fourier transform (FFT) analyzer and a high-speed personal computer-based data acquisition system to perform analysis and calculations of dynamic behavior and flow statistics, as shown in Fig. 1. The data acquisition system had a sample-and-hold function installed for multichannel acquisition

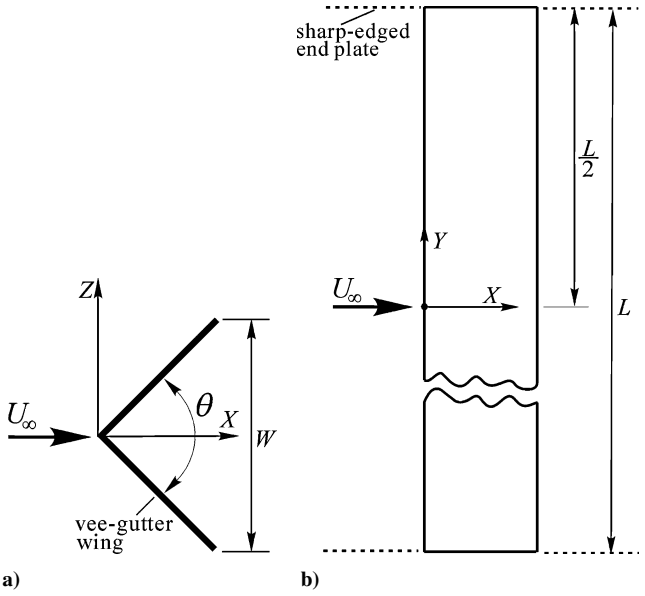

Fig. 2 Geometry of vee gutter: a) top view and b) side view.

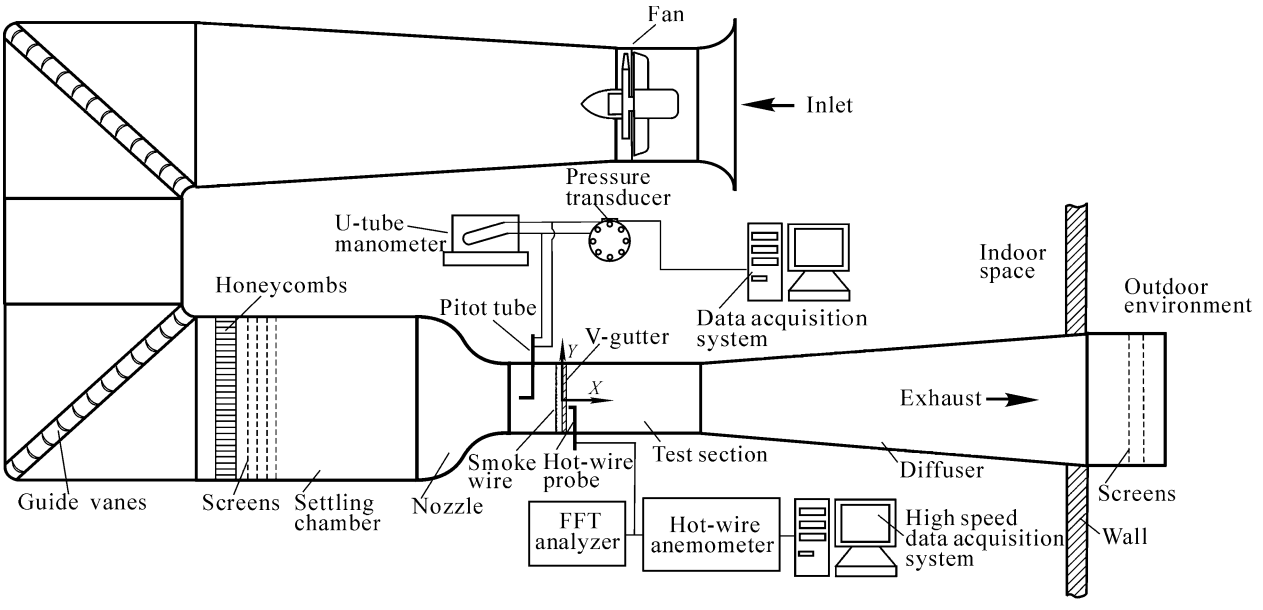

Fig. 1 Experimental set-up.

with no phaselag. The hot-wire probe used was TSI 1210-T1.5, which could be applied in either endflow or crossflow. The original tungsten wire was replaced by platinum wire. The wire diameter and length were 5 μm and 1.5 mm, respectively. The dynamic response corresponding to the electronic square-wave test was adjusted to 20 kHz. The sampling rate and the elapsed time of the data acquisition system were set to 16,000 samples/s and 2 s, respectively, for the measurement of average velocity. They were set to 32,000 samples and 1 s for the freestream turbulence intensity measurements and wakeinstability detection.

The accuracy of the freestream velocity measurement is primarily affected by the alignment of the pitot tube and the calibration of the pressure transducer. With the help of an online micropressure calibration system and careful alignment of the pit tube, the uncertainty of freestream velocity was estimated to be as large as $\pm 1.5\%$ of the reading. The alignment mechanism for the vee gutter has a resolution of ± 0.1 deg. The accuracy of the shedding frequency measurement depends not only on the response of the hot-wire anemometer, but also on the record length and sampling rate of the FFT analyzer. The uncertainty of the frequency detected was estimated to be within $\pm 0.5\%$ of the reading in this experiment.

Results and Discussion

Effective Length

It is well known that the effective span length L_{eff} for cylinder wake measurements usually varies with different clamping conditions at the cylinder ends. To determine the proper dimension and measurement position, a survey of the frequencies of vortex shedding in the wake of the vee gutter of various lengths L was performed at various Reynolds numbers. The data were obtained when the hot wire probe was placed at $(X/W, Z/W) = (4.0, -0.25)$ and the probe was navigated along the Y direction. Figure 3 shows the typical results at $Re_W = 1.9 \times 10^4$. The results are the same for other Reynolds numbers in this experiment, ranging from 0.5×10^4 to 4.0×10^4. The Strouhal number St_W is defined as $St_W = fW/U_\infty$, where f is the shedding frequency, W is the cross-stream width of vee gutter, and U_∞ is the freestream velocity. The Strouhal numbers for all cases of L/W present an almost constant 0.182 within a length centering at about $Y = 0$. Away from the region of constant Strouhal number, the values of the Strouhal numbers decrease rapidly as Y/W goes toward the ends of the vee gutters. The longer the span L of the vee gutter is, the larger the range of the constant Strouhal number appears. When the effective length L_{eff} is defined as the length of the central part of the vee gutter where the Strouhal number decreases by about 10% off its constant value, it is then apparent that for each L/W, there is a corresponding normalized effective length L_{eff}/W across the center $Y/W = 0$, as shown in Fig. 3. Within the range of L_{eff}/W, the Strouhal number St_W remains almost constant at 0.182. Compared with the 0.18 result of Roshko[19] obtained for a 90-deg wedge, the concave geometry of the vee gutter seems to have no significant influence on the instability frequency. The shedding frequency decreases drastically

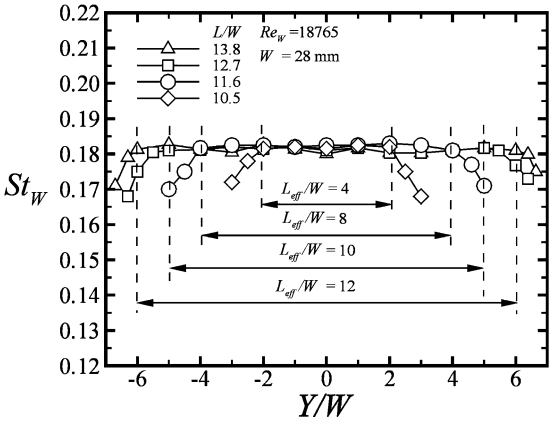

Fig. 3 Effect of span length of vee gutter on vortex shedding frequency in the wake, uncertainty of $St_W = \pm 2.0\%$.

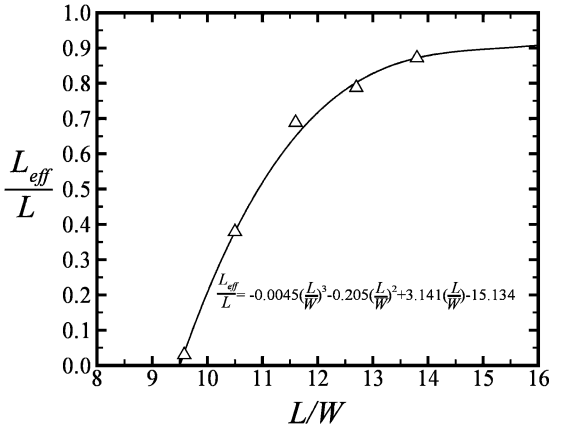

Fig. 4 Normalized effective length of vee gutter, uncertainty of $L_{\text{eff}}/W = \pm 5\%$

when it goes beyond the range of the effective length. The greater the length is, the larger the effective range appears. For instance, at $L/W = 13.8$, the normalized effective length L_{eff}/W is 12, whereas at $L/W = 10.5$, the effective length L_{eff}/W reduces to 4.

Figure 4 shows the variation of the normalized effective length L_{eff}/L with the change of span length L/W. The relationship may be correlated to a third-order polynomial. The effective length L_{eff} may exceed 90% of the span length L when the span length is 15 times greater than the vee-gutter height W. For those which have a span length shorter than about 13, the effective length L_{eff}/L reduces significantly with the decrease of L/W. For $L/W < 9.5$, no effective length can be found. For example, a vee gutter with $L/W = 9.4$ was tested in the laboratory, and no constant frequency section along the span appeared. In the following report, a case of $L/W = 13.8$, which leads to an $L_{\text{eff}}/L = 0.87$, was presented.

Smoke-Streak Flow Pattern

When the smoke-wire flow visualization technique was employed to reveal the flow patterns in the plane $Y/W = 0$, two types of instabilities were observed: the shear-layer instability waves evolving from trailing edges of the wings of vee gutter and the alternative vortex shedding in the wake. Figure 5 shows the typical shear-layer instability waves at various Reynolds numbers. Coherent structures that evolve from the wing trailing edges of the vee gutter are almost symmetric. The size of the roll-ups and the spacing between the coherent structures in the shear layers decrease with the increase of Reynolds number. This implies that the frequency of these shear-layer instabilities increases with the increase of Re_W. For instance, the frequency of the traveling coherent structures at $Re_W = 5.6 \times 10^2$, as shown in Fig. 5a, is about 12 Hz. In contrast, in Fig. 5d for $Re_W = 1.403 \times 10^3$, the instability frequency increases to about 20 Hz. The shear-layer instabilities are hardly observed when the Reynolds numbers are larger than about 1.7×10^3.

Figure 6 shows the time-series pictures of the alternative vortex shedding in the vee-gutter wake at $Re_W = 8.4 \times 10^2$. The nondimensional time t^* is defined as tU_∞/W, where t is the elapsed time. A small upper vortex exists at $t^* = 0$, and a larger lower vortex is located at a distance of about $2W$ downstream the vee gutter. As time elapses, the upper vortex grows, and the lower vortex escapes downstream, as shown in the snapshots of $t^* = 0.93$, 1.86, and 2.79. In the meantime, a new lower vortex grows when the upper vortex escapes successively to complete a cycle, as shown in the streak pictures of $t^* = 2.79$–6.51. If the cycle is estimated by the framing rate, the frequency of the vortex shedding is about 3.75 Hz, which is much lower than that of the shear-layer instabilities.

Characteristic Modes of Instabilities

From the smoke-wire flow visualization pictures, as shown in Figs. 5 and 6, the wake instabilities in the midspan plane behind the veegutter are identified as the shear-layer instability and vortex shedding. The shear-layer instabilities, which are small convective

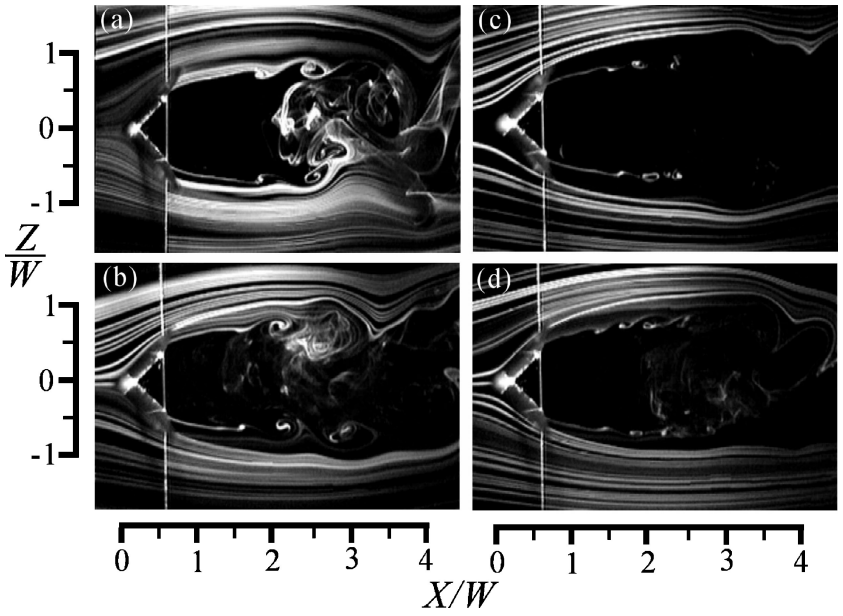

Fig. 5 Instantaneous pictures of coherent structures in shear layers evolving from trailing edges of vee gutter, $W = 28$ mm, and exposure time = 1/2000 s: a) $Re_W = 5.6 \times 10^2$, b) $Re_W = 9.33 \times 10^2$, c) $Re_W = 1.168 \times 10^3$, and d) $Re_W = 1.403 \times 10^3$, uncertainty of $Re_W = \pm 1.5\%$.

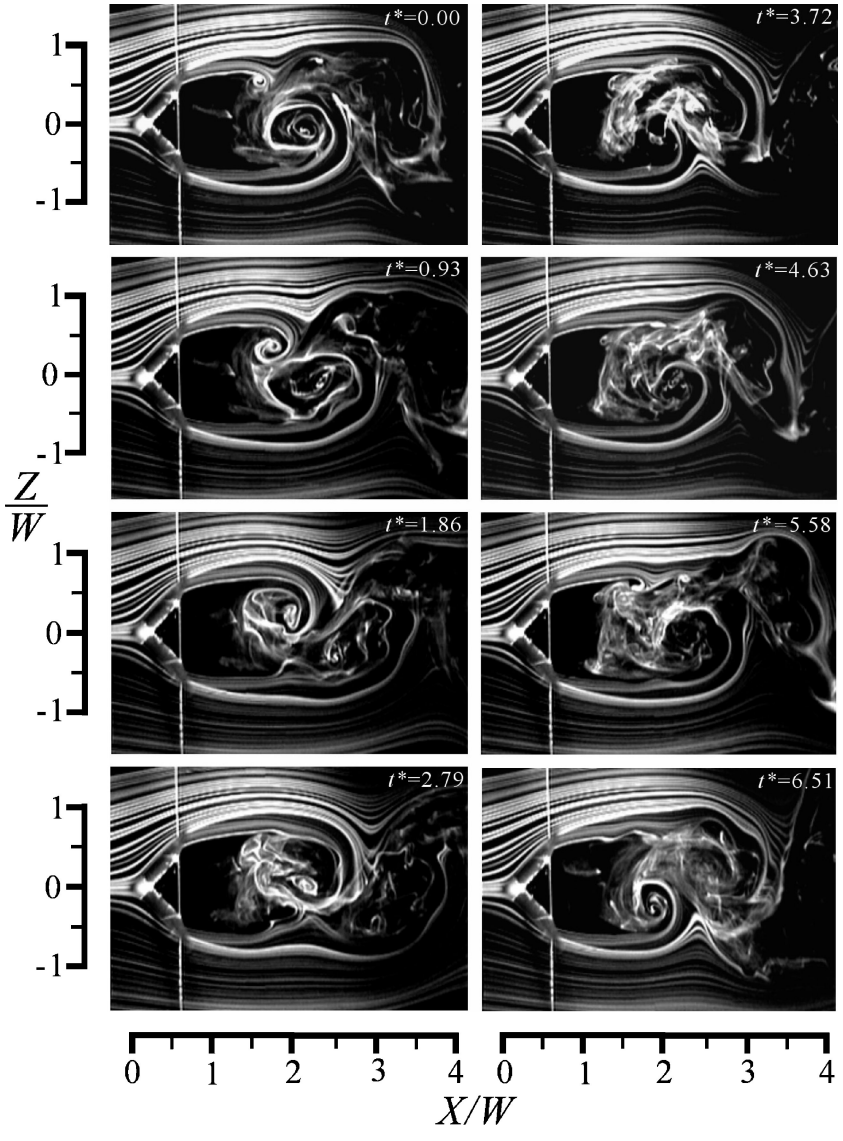

Fig. 6 Stream pictures of vortex shedding in near wake region: $W = 28$ mm, exposure time = 1/2000 s, $Re_W = 8.4 \times 10^2$, uncertainty of $Re_W = \pm 1.5\%$.

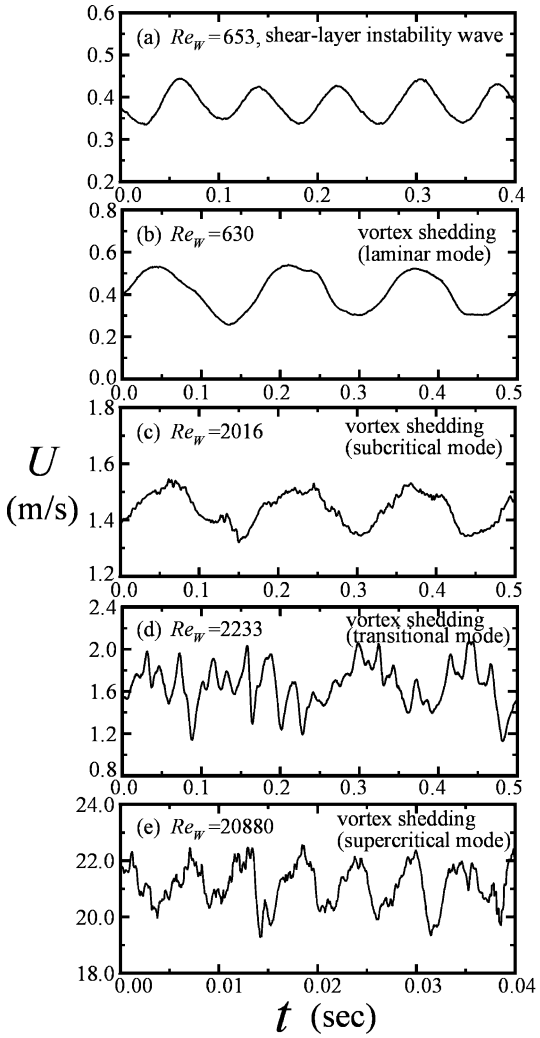

Fig. 7 Time series of hot-wire anemometer signals of instabilities in various Reynolds number regimes: a) shear-layer instability wave, b) laminar mode vortex shedding, c) subcritical mode vortex shedding, d) transitional mode vortex shedding, and e) supercritical mode vortex shedding, uncertainty of velocity U is ±1.5%.

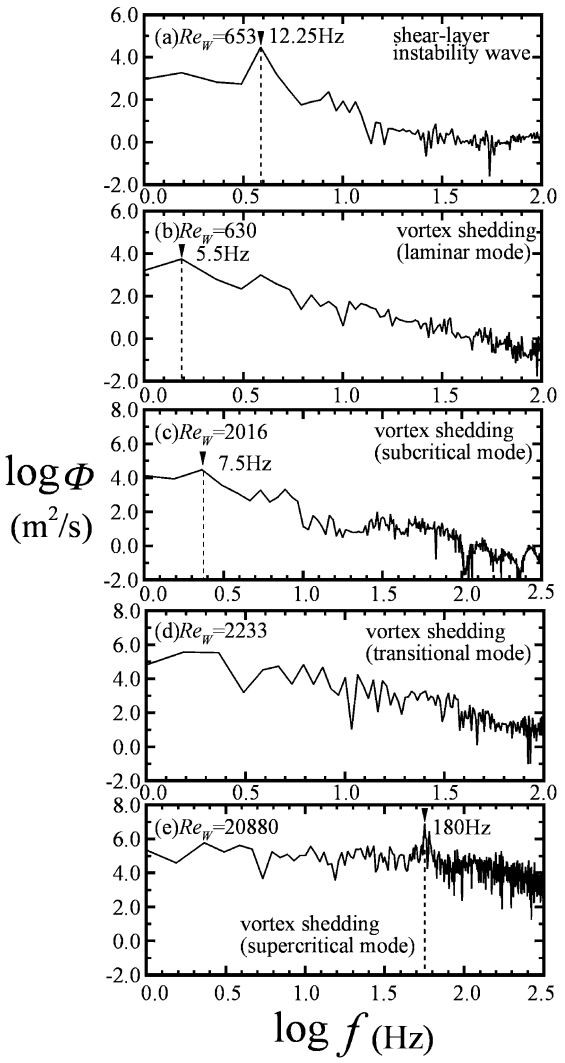

Fig. 8 FFT transformed frequency domain corresponding to Fig. 7, uncertainty of frequency f is ±0.5%.

coherent structures induced by the shear effect, evolve from the trailing edge of the vee gutter. In contrast, the vortex sheddings, which are the large roll-ups induced by the unsteady inertial or pressure effect, are alternatively released in the wake. By application of the hot-wire anemometer to the shear layer and the wake, oscillating signals of the shear-layer instability waves and the vortex shedding, respectively, are detected. Figure 7 shows the typical hot-wire signals of the instability waves in the shear layer (Fig. 7a) and the vortex shedding in the wake (Figs. 7b–7e). The shear-layer instability signals are detected at $(X/W, Z/W) = (3.0, -0.5)$, whereas the vortex shedding signals are obtained at $(X/W, Z/W) = (4.0, -0.25)$.

At $Re_W = 6.53 \times 10^2$, as shown in Fig. 7a, the periodic signals detected by the hot-wire anemometer contain low-amplitude oscillations (±0.05 m/s about its center value) of the ac component. The frequency of the periodic motion is 12.25 Hz, as shown in the power spectrum of Fig. 8a. Figure 8 is obtained from the corresponding time domain data of Fig. 7 by the use of the digital FFT technique.[28] The shear-layer instability waves can not be detected when Re_W is greater than about 1.7×10^3.

At $Re_W = 6.3 \times 10^2$, as shown in Fig. 7b, the hot-wire probe positioned at $(X/W, Z/W) = (4.0, -0.25)$ detects a periodic oscillating signal. The frequency of oscillation, as shown in Fig. 8b, is 5.5 Hz. It is lower than the shear-layer signal of Fig. 7a. The amplitude of oscillations (±0.16 m/s about its center value), however, is larger than the shear-layer signal of Fig. 7a. The signals of the oscillations are relatively smooth, which corresponds to the laminar mode of vortex shedding found by Lienhard[29] in the circular-cylinder wake and by Huang and Lee[18] in the wing wake. This type of vortex shedding is expected to be observed in the range $Re_W < 1.2 \times 10^3 \pm 20$.

Figure 7c shows the vortex shedding signals at $Re_W = 2.016 \times 10^3$. The oscillating signals are superimposed by fluctuations. Although the Reynolds number is increased by about 3.2 times that of Fig. 7b, the frequency in the corresponding power spectrum of Fig. 8c is slightly increased to 7.5 Hz. The slight fluctuations superimposed on the low-frequency oscillations of the hot-wire signals imply that turbulence motions appear in the shed vortices. The vortex shedding of this type is termed the subcritical mode. It occurs when the Reynolds number is pushed up across about $1.2 \times 10^3 \pm 20$ and below $2.1 \times 10^3 \pm 25$. The turbulent fluctuations develop with the spatial evolution of shedding vortices. The intensity of the turbulent fluctuations amplifies, and the periodicity of the vortex shedding decreases with the increase of the Reynolds number.

When the Reynolds number ranges between $2.1 \times 10^3 \pm 25$ and $2.35 \times 10^3 \pm 20$, random fluctuations appear in the signal of hot-wire anemometer, as typically shown in Fig. 7d for $Re_W = 2.233 \times 10^3$. The periodic signals as shown in the laminar and subcritical modes are no longer observed. Wake flows of this type are in what is termed the transitional mode. No particular peak is found in the power spectrum of the velocity signals, as shown in Fig. 8d. The shed vortices lose coherency, and the flow structure in the wake is disorganized, probably due to the mixing effect induced by the increased turbulence intensity.

Table 1 Reynolds numbers of characteristic vortex shedding modes

Bluff body	Characteristic vortex shedding mode			
	Laminar	Subcritical	Transitional	Supercritical
Circular cylinder[29]	$Re < 300$	$300 < Re < 3 \times 10^5$	$3 \times 10^5 < Re < 3.5 \times 10^6$	$Re > 3.5 \times 10^6$
NACA0012 wing at 5 deg angle of attack[18]	$Re < 3500$	$3500 < Re < 5000$	$5000 < Re < 1.7 \times 10^4$	$Re > 1.7 \times 10^4$
Vee gutter of 90-deg span angle (present work)	$Re < 1200$	$1200 < Re < 2100$	$2100 < Re < 2350$	$Re > 2350$

When the Reynolds number is greater than $2.35 \times 10^3 \pm 20$, periodic hot-wire signals are present again. The signals, however, are typically superimposed by large turbulent fluctuations, as shown in Fig. 7e for $Re_W = 2.088 \times 10^4$, which indicates that turbulent vortices are shed in the wake. A peak at $f = 180$ Hz in the power spectrum is observed again, as shown in Fig. 8e. The vortex shedding of this type is termed the supercritical mode.

The behaviors of vortex shedding in the vee-gutter wake are compared with those found in the circular-cylinder wake[29] and the wing wake[18], as shown in Table 1. The mode change of vortex shedding in the circular-cylinder wake[29] is closely related to the behaviors of boundary layer on the cylinder surface. The subcritical vortices are observed in a wide range of Reynolds numbers between 3×10^2 and 3×10^5, which are induced by the propagation of instabilities of the vortical structures. The famous almost constant Strouhal law (Strouhal number ≈ 0.21) dominates in this range. The transitional wake, where the vortex shedding disappears, occurs in the range of Reynolds numbers between 3×10^5 and 3.5×10^6 when the laminar boundary layer on the solid surface undergoes a transition to turbulence. The supercritical vortex shedding appears as the Reynolds number is greater than 3.5×10^6, when the boundary layer on the solid wall becomes turbulent. In this range, the Strouhal number increases with the increase of Reynolds number. The behaviors of vortex shedding occurring in the wing wake[18] depend on the Reynolds number, angle of attack, and freestream turbulence. Mode change is closely related to the propagation of instabilities and separation and reattachment of boundary layers. The range of Reynolds numbers where the transition occurs covers about 10^4. In the present case, boundary-layer separation on the vee-gutter walls cannot occur because of the positive pressure gradient. The transition is observed in a narrow range of Reynolds numbers from 2.1×10^3 to 2.35×10^3. It seems that sharp edges of the bluff body will trigger the instabilities of the shed vortices and cause early transition of the vertex shedding. The ranges of the vortex shedding modes may differ when the bluff-body curvatures are varied. The fundamental behaviors, however, are similar.

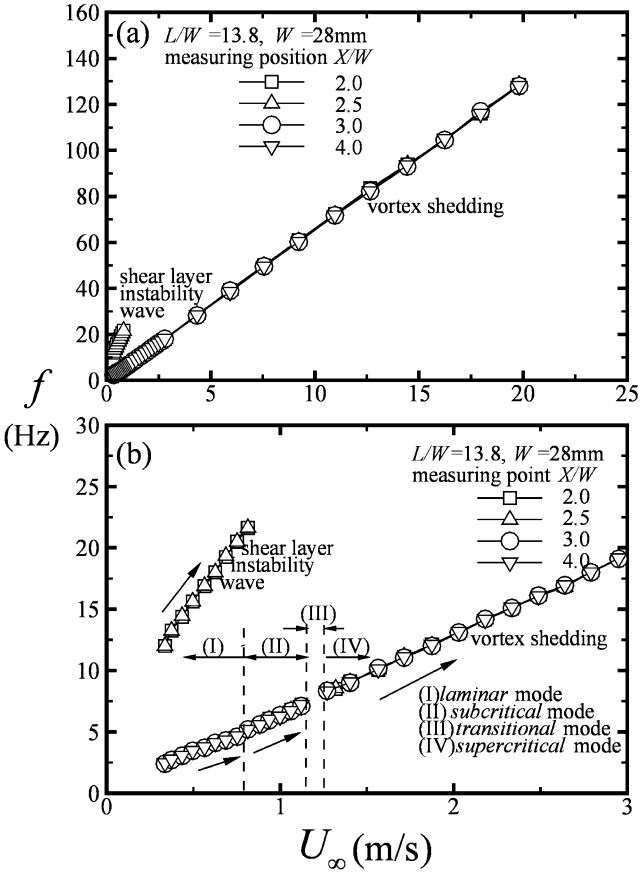

Fig. 9 Frequency variations of shear-layer instabilities and vortex shedding in the wake, uncertainty of frequency f is $\pm 0.5\%$. uncertainty of velocity U is $\pm 1.5\%$.

Frequency Characteristics

The frequencies of the periodic unsteady motions in the shear layer and the wake, which vary with the freestream velocity, are shown in Fig. 9. In Fig. 9a, the frequencies of the shear-layer instability waves and the vortex shedding increase linearly with the increase of the freestream velocity. The shear-layer instability waves can be detected only at the velocities lower than about 0.9 m/s, where higher oscillation frequencies than those of vortex shedding at corresponding wind velocities are apparently found. Figure 9b reveals the details in the range $U_\infty < 3$ m/s. The increase rate of the vortex shedding frequency in the laminar mode is a little lower than those in the subcritical and supercritical modes. No oscillation frequency is detected in the transitional range, in this case, no data point appears there.

With account taken of the similarity theory[30] and the balance of the order of magnitudes between the unsteady term and the inertial term in the Navier–Stokes equation, it may be justified that the nondimensional variable fW/U_∞, which was conventionally called the Strouhal number St_W, has to approach a constant in the limiting case of large Reynolds numbers.[31] In other words, in the inertial-dominated range, where the viscosity effect is insignificant, $St_W \rightarrow$ constant. On the other hand, when the unsteady term and the viscous term in the Navier–Stokes equation are balanced, another nondimensional variable fW^2/ν, which was conventionally called the Roshko number Ro_W, has to approach a constant.[31] That is, in the viscous-effect dominated regime, for example, at very low Re_W, $Ro_W \rightarrow$ constant. There is a relationship between the dimensionless groups, Re_W, St_W, and Ro_W, that is,

$$ReW = U_\infty W/\nu = (fW^2/\nu)/(fW/U_\infty) = Ro_W/St_W \qquad (1)$$

Hence, when the instabilities in the wake are considered, Ro_W will be proportional to Re_W in the inertial-dominated regime, and St_W will be inversely proportional to Re_W in the viscosity-dominated regime, as shown in Fig. 10.

The results are shown in Fig. 11 for when the frequencies of the periodic unsteady motions in the wake, which may vary with the wind velocity, are normalized and represented by the Strouhal number $St_W = fW/U_\infty$. The Strouhal number of the shear-layer instability waves decreases nonlinearly from 1.0 to 0.75 as the Reynolds number increases from 6.2×10^2 to 1.5×10^3. The Roshko number of the shear-layer instability waves, which can be obtained by multiplication of the corresponding St_W to Re_W, is not a constant. It is an increasing function of the Reynolds number. The decreasing Strouhal number implies that the shear-layer instability waves are subject to both the influences of viscosity and inertia. The inertia

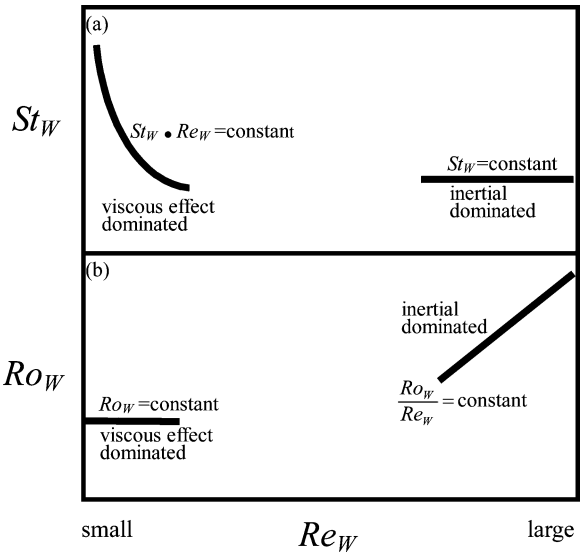

Fig. 10 Asymptotic behaviors of Strouhal number and Roshko number.

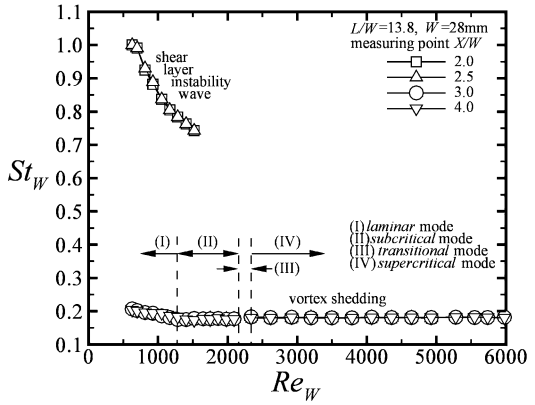

Fig. 11 Strouhal numbers of shear-layer instabilities and vortex shedding in the wake, uncertainty of $St_W = \pm 2.0\%$.

is not a sole dominant factor for the formation mechanism of the shear-layer coherent structures.

The Strouhal number of the vortex shedding is much lower than that of the shear-layer instability wave. In the regime of laminar vortex shedding, St_W decreases slightly from 0.21 to 0.182 as the Reynolds number increases from 6.2×10^2 to 1.2×10^3. In the regimes of subcritical and supercritical modes, the Strouhal number remains at an almost constant 0.182. The slight decrease of the Strouhal number in the laminar mode indicates that the viscosity still presents some effects on the instability behavior of the vortex shedding in this regime. However, the inertial force of the oscillations in the shed vortices plays a more important role than it does in the shear-layer instability waves. The total domination of the inertial occurs when the Reynolds number is large enough to be in the subcritical and supercritical regimes.

Effect of Cross-Stream Width and Trailing-Edge Sharpness

In the subcritical or supercritical mode, the Strouhal numbers remain at almost the same value. The value of constant Strouhal number varies with the shape and the sharpness of the body. Table 2 shows the statistics of several conditions. The Strouhal number measured in the wake behind a circular cylinder at large Reynolds numbers between 10^3 and 10^5, which are based on the cylinder diameter, is about 0.21 (Ref. 29). For a NACA 0012 wing section, it is 0.21 and 0.12 at 15- and 90-deg angle of attack, respectively. The Strouhal number for a vertically aligned, thick, square-edged flat plate[32] and sharp-edged flat plate[33] is 0.15 and 0.13, respectively. It is expected that sharpened trailing edges and bluffed blockage in the crossflow would lead to a smaller Strouhal number. For a sharp-edged bluff body, the Strouhal number of the vortex shedding would approach a lower limit of about 0.12. The value 0.12 is less than the universal Strouhal number 0.159 obtained theoretically by Levi[21] for a bluff body because the physical dimension of the blockage, instead of the wake width, is employed in calculating the Strouhal number.

Table 2 Strouhal numbers of varies bluff bodies

Bluff body	St_W of subcritical or supercritical mode
NACA0012 wing[18]	0.44 at 5-deg angle of attack
Circular cylinder[29]	0.21
NACA0012 wing[22,18]	0.20 at 16-deg angle of attack
90-deg vee gutter with square-edged trailing edges (present work)	0.182
Vertically aligned, thick, square-edged flat plate[31]	0.15
Vertically aligned, thick, sharp-edged flat plate[32]	0.13
NACA0012 wing[18]	0.12 at 90-deg angle of attack

Conclusions

The oscillating behaviors of the unsteady flows in the wake of a vee gutter are studied. The effective length may exceed 90% of the span length when the span length is 15 times greater than the vee-gutter height. For those, which have a span length shorter than a 9.5 cross-stream width, no effective length can be found. This result is consistent with the conventional notion that the aspect ratio must be larger than about 10 to simulate a two-dimensional flowfield. The oscillating flowfield in the wake region of the vee gutter exhibits the characteristics of two instabilities: the high-frequency shear-layer instability waves and the low-frequency vortex shedding. Four characteristic modes: laminar, subcritical, transitional, and supercritical, are identified in the shed vortices. The shear-layer instability waves and the laminar vortical shedding are observed at low Reynolds numbers. Their formations are closely related to the viscous effect. The Strouhal number in this viscosity effective regime decreases with the increase of Reynolds number. No periodic frequency is found in the transitional wake. The vortex shedding observed in the subcritical and supercritical wakes are superimposed by turbulence fluctuations. The Strouhal number approaches a constant 0.182 in these inertial dominated regimes. Similarity analysis justifies that the Strouhal number and the Roshko number have to approach constants at very high and low Reynolds number regimes, respectively. By comparison of the various results of wake experiments, it is expected that sharpened trailing edges and bluffed blockage in the crossflow would lead to a smaller Strouhal number.

References

[1]Hertzberg, J. R., Shepherd, I. G., and Talbot, "Vortex Shedding Behind Rod Stabilized Flames," *Combustion and Flame*, Vol. 86, No. 1, 1991, pp. 1–11.

[2]Popiel, C. O., and Turner, J. T., "Visualization of High Blockage Flow Behind a Flat Plate in a Rectangular Channel," *Journal of Fluids Engineering*, Vol. 113, No. 1, 1991, pp. 143–146.

[3]Beer, J. M., and Chigier, N. A., "Modeling of Double Concentric Burning Jets," *Ninth Symposium (International) on Combustion*, Academic, New York, 1963, pp. 892–900.

[4]Roquemore, W. M., Tankin, R. S., Chiu, H. H., and Lottes, S. A., "A Study of a Bluff-Body Combustor Using Laser Sheet Lighting," *Experiments in Fluids*, Vol. 4, No. 4, 1986, pp. 205–213.

[5]Fujii, S., and Eguchi, K., "A Comparison of Cold and Reacting Flows Around a Bluff-Body Flame Stabilizer," *Journal of Fluids Engineering*, Vol. 103, No. 2, pp. 328–334.

[6]Fujii, S., Gomi, M., and Eguchi, K., "Cold Flow Tests of a Bluff-Body Flame Stabilizer," *Journal of Fluids Engineering*, Vol. 100, No. 3, 1978, pp. 323–332.

[7]Stwalley, R. M., and Lefebvre, A. H., "Flame Stabilization Using Large Flameholders of Irregular Shape," *Journal of Propulsion*, Vol. 4, No. 1, 1988, pp. 4–13.

[8]Yang, J. T., Tsai, G. L., and Wang, W. B., "Near-Wake Characteristics of Various V-Shaped Bluff-Body," *Journal of Propulsion and Power*, Vol. 10, No. 1, 1994, pp. 288–294.

[9]Yang, J. T., Yen, C. W., and Tsai, G. L., "Flame Stabilization in the Wake Flow Behind a Slit V-Gutter," *Combustion and Flame*, Vol. 99, No. 2, 1994, pp. 288–294.
[10]King, R., "A Review of Vortex Shedding Research and Its Application," *Ocean Engineering*, Vol. 4, No. 3, 1977, pp. 141–171.
[11]Griffin, O. M., "Universal Similarity in the Wakes of Stationary and Vibrating Bluff Structures," *Journal of Fluids Engineering*, Vol. 103, No. 1, 1981, pp. 52–58.
[12]Griffin, O. M., "Vortex Shedding from Bluff Bodies in a Shear Flow: A Review," *Journal of Fluids Engineering*, Vol. 107, No. 3, 1985, pp. 298–306.
[13]Motallebi, F., and Norbury, J. F., "The Effect of Base Bleed on Vortex Shedding and Base Pressure in Compressible Flow," *Journal of Fluid Mechanics*, Vol. 110, 1981, pp. 273–292.
[14]Vassilopoulos, K., Gai, S. L., and Petrusma, M. S., "Unsteady Flow Behind a Blunt Trailing Edge Aerofoil," AIAA Paper 95-0531, 1995.
[15]Brooks, T. F., and Schlinker, R. H., "Progress in Rotor Broadband Noise Research," *Vertica*, Vol. 7, 1983, pp. 287–307.
[16]Stuber, K., and Gharib, M., "Experiment on the Forced Wake of an Airfoil Transition from Order to Chaos," AIAA Paper 88-3840 CP, 1988, pp. 723–730.
[17]Huang, R. F., and Lin, C. L., "Vortex Shedding and Shear-Layer Instability of Wing at Low Reynolds Numbers," *AIAA Journal*, Vol. 33, No. 8, 1995, pp. 1398–1430.
[18]Huang, R. F., and Lee, H. W., "Turbulence Effect on Frequency Characteristics of Unsteady Motions in Wake of Wing," *AIAA Journal*, Vol. 38, No. 1, 2000, pp. 87–94.
[19]Roshko, A., "On the Wake and Drag of Bluff Bodies," *Journal of the Aerospace Sciences*, Vol. 22, Feb. 1955, pp. 124–135.
[20]Simons, J. E. L., "Similarities Between Two-Dimensional and Axisymmetric Vortex Wakes," *Aeronautical Quarterly*, Vol. 26, 1977, pp. 15–20.
[21]Levi, E., "A Universal Strouhal Law," *ASCE Journal of Engineering*, Vol. 109, Nov. 1983, pp. 718–727.
[22]Zaman, K. B. M. Q., McKinzie, D. J., and Rumsey, C. L., "A Natural Low-Frequency Oscillation of the Flow Over an Airfoil Near Stalling Conditions," *Journal of Fluid Mechanics*, Vol. 202, 1989, pp. 403–442.
[23]Oertel, H., Jr., "Wakes Behind Blunt Bodies," *Annual Reviews of Fluid Mechanics*, Vol. 22, 1990, pp. 539–564.
[24]Nishioka, M., and Sato, H., "Mechanism of Determination of the Shedding Frequency of Vortices Behind a Cylinder at Low Reynolds Numbers," *Journal of Fluid Mechanics*, Vol. 89, 1978, pp. 49–60.
[25]Bejan, A., *Convective Heat Transfer*, Wiley, New York, 1984, pp. 110–114.
[26]Muller, T. J., "Flow Visualization by Direct Injection," *Fluid Mechanics Measurements*, 2nd ed., edited by R. J. Goldstein, Taylor and Francis, London, 1996, pp. 367–450.
[27]Flagan, R. C., and Seinfeld, J. H., *Fundamentals of Air Pollution Engineering*, Prentice–Hall, Englewood Cliffs, NJ, 1988, pp. 295–307.
[28]McGillem, C. D., and Cooper, G. R., *Continuous and Discrete Signal and System Analysis*, 2nd ed., Holt, Rinehart, and Winston, New York, 1983, pp. 163–200.
[29]Lienhard, J. H., "Synopsis of Lift, Drag, and Vortex Frequency Data for Rigid Circular Cylinders," College of Engineering, Research Divi. Bulletin 300, Washington State Univ., Pullman, WA, 1966.
[30]Gukhman, A. A., *Introduction to the Theory of Similarity*, Academic, New York, 1965, pp. 19–44.
[31]Lee, H. W., "The Flows on the Suction Surface and Instability Motions in the Wake of a Wing," Ph.D. Dissertation, Dept. of Mechanical Engineering, National Taiwan Univ. of Science and Technology, Taipei, Taiwan, Republic of China, June 1999.
[32]Novak, J., "Strouhal Number and Flat Plate Oscillation in an Air Stream," *Acta Technica Csav*, Vol. 4, July 1973, pp. 372–386.
[33]Toebes, G. H., and Eagleson, P. S., "Hydroelastic Vibrations of Flat Plates Related to Trailing Edge Geometry," *Journal of Basic Engineering*, Vol. 83, No. 4, 1961, pp. 671–678.